Adv. Polar Upper Atmos. Res., **14**, 55–65, 2000

Generation region of polar cusp hiss observed by ISIS satellites

Tadanori Ondoh

Space Earth Environment Laboratory, Kitano, Tokorozawa 359-1152

Abstract: Polar cusp VLF hiss of irregular spectra is observed mainly at geomagnetic invariant latitudes from 74° to 84°, and at geomagnetic local times from 10 to 14 hours. This occurrence region corresponds well to a region of cusp precipitations of low-energy electrons below 1 keV. Changes of lower cutoff frequency of polar cusp hiss are related with plasma irregularities in the polar cusp ionosphere. The whistler-mode Cerenkov radiation from electrons below 1 keV is discussed for generating the polar cusp hiss, but this mechanism can not work in the polar cusp ionosphere for VLF frequencies much lower than a local electron gyrofrequency. The whistler-mode VLF Cerenkov radiation is generated from the electrons below 1 keV at high altitude(~6 R_E) cusp magnetosphere, where a local electron gyrofrequency is in VLF band. The whistler-mode cusp hiss generated at high altitudes will propagate along field-aligned cusp plasma down to a strong geomagnetic field region where the cusp structure fades out. Below this region, the whistler-mode hiss spreads over the polar cusp ionosphere where low energy electron precipitations produce ionospheric irregularities.

1. Introduction

There have been hitherto published a few papers on satellite observations of polar cusp VLF emissions. Gurnett and Frank (1978) first observed ELF-ULF magnetic noises and whistler-mode hiss at invariant latitudes of 76°–82° in high altitude cusp region. Irregular spectra of polar cusp hiss in the topside ionosphere were reported by Ondoh *et al.* (1981) and Ondoh (1997). Ondoh (1997) has reported that an occurrence region of polar cusp VLF emissions observed by ISIS satellites agrees with a precipitation region of polar cusp low energy electrons (500 eV–1 keV) between 10 and 16 MLT and between 67° and 82° invariant latitude (Carbary and Meng, 1986a).

Figure 1 shows fine intensity variations in 5 and 8 kHz narrow-bands in the polar cusp region observed by ISIS-1 on April 12, 1978. Fine intensity variations are spatial ones in longitude, because the MLT changed widely from 14 to 11 MLT for 3 min in UT along satellite orbit. Enhanced coarse intensity variations outside the upward arrows show occurrences of stable auroral hiss. Since the geomagnetic axis inclines 11.7° to the earth's rotation axis, a high latitude part of the satellite polar orbit is often along the latitudinal circle. Hence, the ISIS satellites had chances to observe the polar cusp hiss for several hours in MLT for a few minutes in UT.

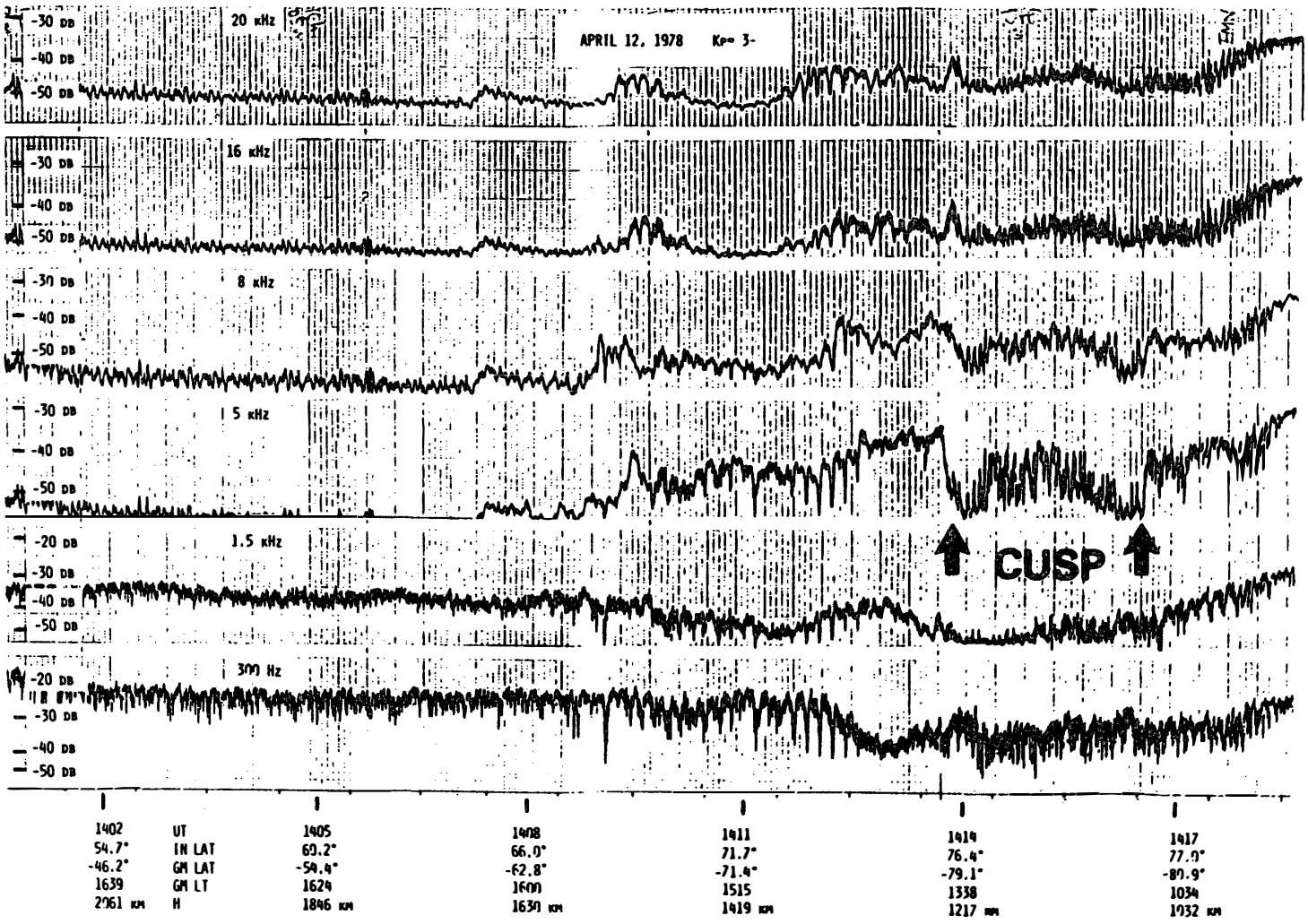

Fig. 1. Fine intensity variations of polar cusp hiss at 5 and 8 kHz bands between two upward arrows observed by ISIS-1 on April 12, 1978, K_p=3–.

2. Inherent characteristics of polar cusp hiss observed in the cusp ionosphere

Figures 2a and 2b show *f-t* spectra of polar cusp hiss corresponding to the fine intensity variations at 5 kHz band between two arrows indicated in Fig. 1. A linear frequency scale is from dc to 10 kHz and a linear time scale is 30 s from the left to the right end in Figs. 2a–2b. The top panel of Fig. 2a shows the end of stable auroral hiss at invariant latitude 76.0°. But all panels from the second one in Fig. 2a to the bottom of Fig. 2b show irregular spectra of polar cusp hiss corresponding to the fine intensity variations at 5 and 8 kHz bands in Fig. 1. The latter half spectra of the bottom panel in Fig. 2b show again an auroral hiss with a steady lower frequency cutoff around 2 kHz, indicating that the ISIS-1 left the polar cusp region at 1417 UT (inv. lat. 77.0°, 1034 MLT) and moved westward along a latitudinal circle of 77°. Thus, the polar cusp hiss appeared between regions of the auroral hiss regions. Hourly values of auroral electrojet indices in the period of polar cusp hiss on April 12, 1978 were AE=73 nT and AL=–34 nT at 13 UT, AE=86 nT and AL=–41 nT at 14 UT, and AE=278 nT and AL=–173 nT at 15 UT (Kamei and Maeda, 1981); the polar cusp hiss in Fig. 2 occurred in a geomagnetic quiet period. Upper and lower panels in Fig. 3 show respectively invariant latitude and geomagnetic local time distributions of the occurrence rate of polar cusp hiss obtained from 76 ISIS passes between June 1976 and August 1978 at Syowa Station. The polar cusp hiss occurs mainly at invariant latitudes from 74° to 84°, and between 9 and 15 MLT. High occurrence rates of the polar cusp hiss lie at invariant latitudes from 76° to 80° and from 11 to 13 MLT. Figure 4 shows locations of all polar cusp signatures for low energy electrons below 1 keV observed by DMSP-F2 and -F4 during February–December, 1979, where 222 events marked by crosses denote those observed in the southern hemisphere, and 150 events in the northern hemisphere are shown with triangles (Carbary and Meng, 1986a). The distribution of the polar cusp hiss in Fig. 3 is very similar to that of the polar cusp signatures for low energy electrons in Fig. 4. This similarity implies that the polar cusp hiss is generated from the low energy electrons precipitating into the polar cusp ionosphere.

3. Variations of lower cutoff frequency for polar cusp hiss

Since the polar cusp hiss and auroral hiss observed in the ionosphere are whistler-mode waves with large wave normal angles to the geomagnetic field, they have large electric fields in the wave normal direction. Non-ducted VLF waves are reflected at a frequency slightly lower than the local LHR frequency at wave normal perpendicular to local geomagnetic field (Kimura, 1966). Hence, waves of polar cusp hiss and auroral hiss near the LHR frequency spend a long time compared with crossing times of waves passing around the reflection region. The electric field in the wave normal direction of non-ducted VLF waves is very strong near the LHR frequency, as seen at the lower cutoff frequency of polar cusp hiss in Fig. 2. The lower hybrid resonance frequency, f_{LHR} is given by $f_{LHR}^2=Cf_H^2\, f_P^2/(f_H^2+f_P^2)$, $C=m_e/[m_P\cdot m(\mathrm{eff})]$, where f_H is the electron gyrofrequency, f_P the electron plasma frequency, m_P the proton mass, and m_e the electron mass. Since the effective mean ionic mass number in the polar ionosphere is m(eff)=8,

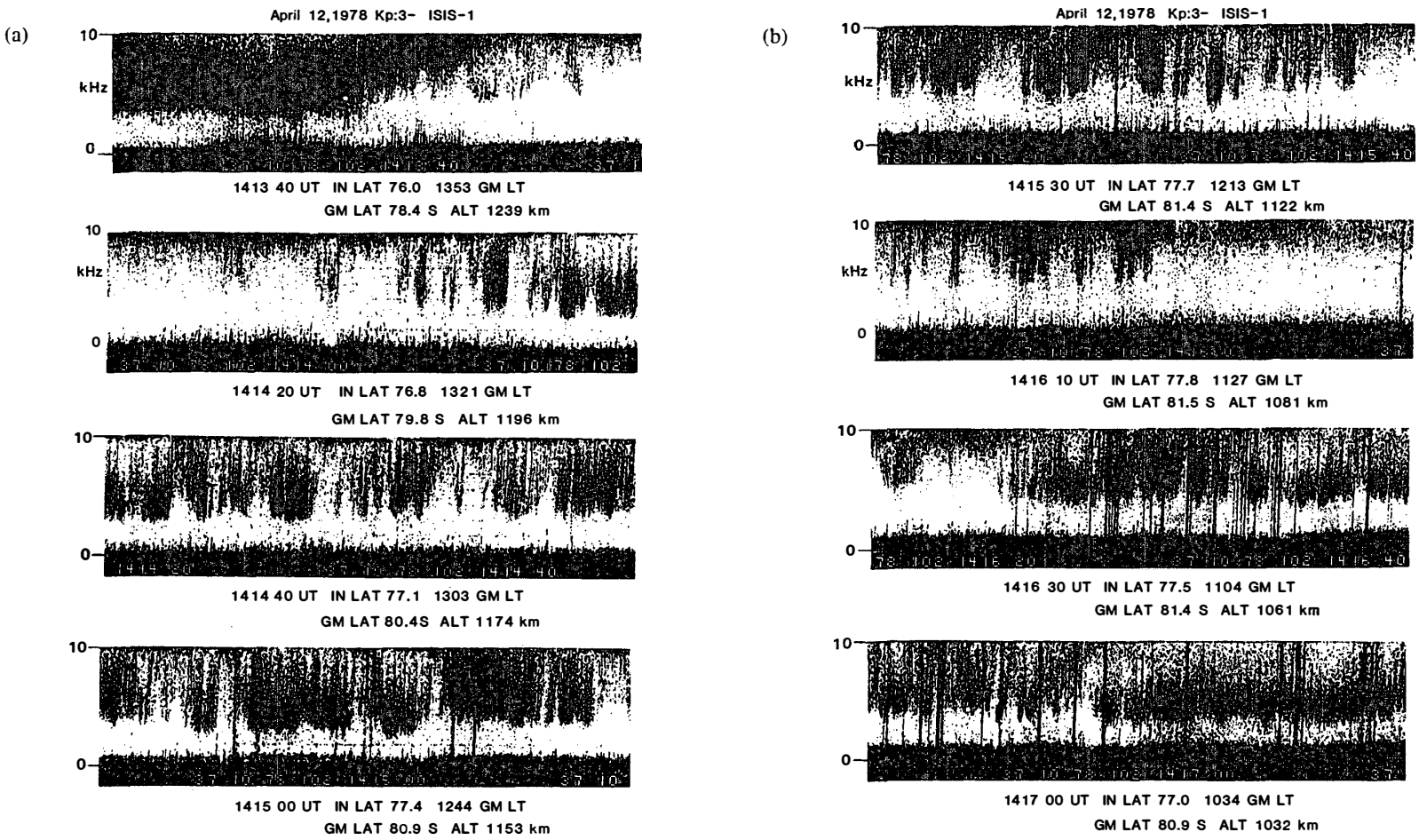

Figs. 2a-2b. Irregular f-t spectra of polar cusp hiss observed by ISIS-1 on April 12, 1978. Top panel in Fig. 2a and bottom panel in Fig. 2b show steady lower cutoff frequency of drape-like auroral hiss, respectively.

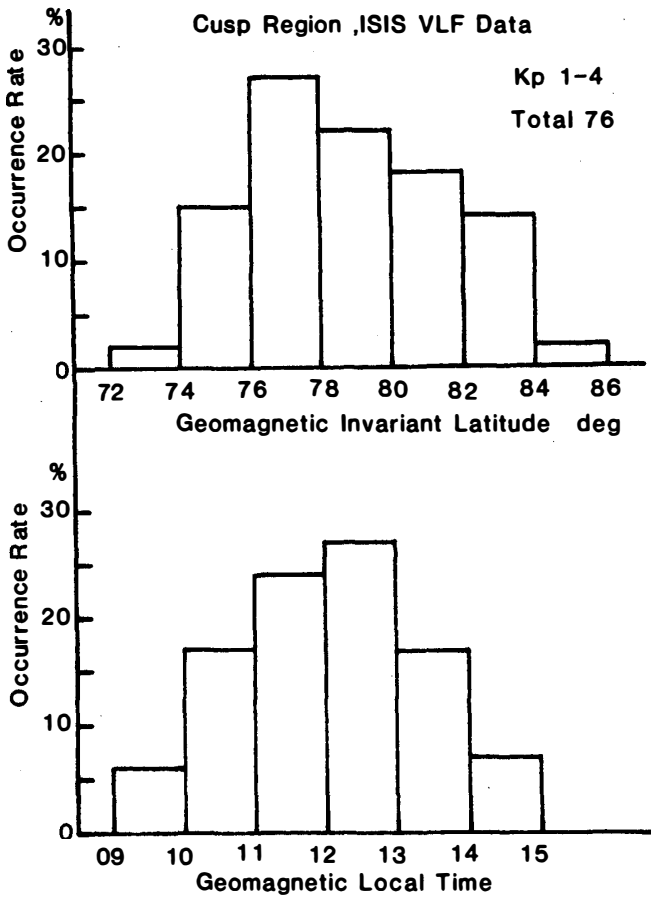

Fig. 3. Statistical distributions of polar cusp hiss in geomagnetic invariant latitude (upper half) and in geomagnetic local time (lower half) obtained from 76 ISIS VLF passes received at Syowa Station, Antarctica from June 1976 to August 1978.

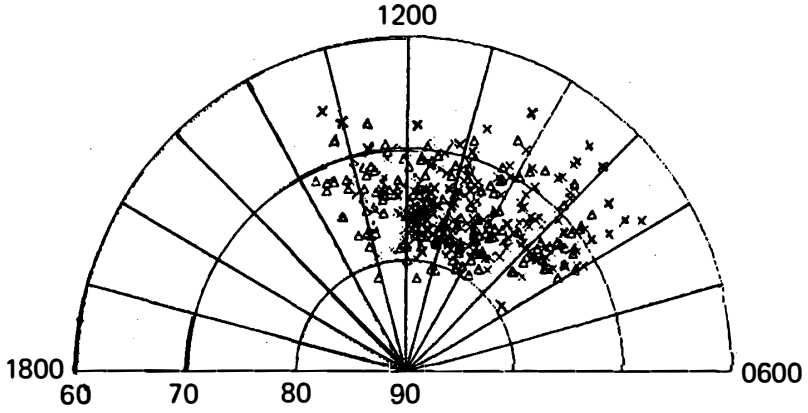

Fig. 4. Locations of all polar cusp signatures for low-energy electrons in geomagnetic latitude and local time, detected by DMSP satellites for February-December 1979, where 220 crosses and 150 triangles were observed in the southern and northern hemispheres, respectively (Carbary and Meng, 1986a).

f_{LHR}=1–8 kHz and f_H=972 kHz at 1410 km of geomagnetic latitude 80°, we have $f_P^2 = f_{LHR}^2/[C-(f_{LHR}/f_H)^2]$ and $f_P^2 \simeq f_{LHR}^2/C$ for $f_H^2 \gg f_{LHR}^2$ in the polar ionosphere. The last expression gives $N/cm^3 = 181.3\, f_{LHR}^2$. A typical cusp hiss in Fig. 2 shows a steady lower cutoff frequency (~2 kHz) lasting for 2 s and a rapid rise of frequency in 1 s. The f_{LHR} changes from 2 kHz ($N = 725/cm^3$) to 7.5 kHz ($10^4/cm^3$) for 3 s. This change shows a spatial dependence of the polar cusp hiss along the satellite orbit of Fig. 3. If *f-t* spectra of cusp hiss depend on a structure of a plasma cavity, the lower cutoff frequency is low (2 kHz) at the center of plasma cavity and high (7.5 kHz) at the cavity edges. A plasma density depression at the cusp hiss center is $\Delta N/N \sim -0.9$ on spatial scale of 24 km at satellite speed of 8 km/s in the polar cusp ionosphere.

4. Structure of magnetospheric cusp region

The total geomagnetic flux over the whole polar cap is $2B_0\pi R_E^2\cos^2\theta_C$ where B_0=3.0×10^4 nT is the geomagnetic flux at the ground geomagnetic equator, θ_C is the geomagnetic latitude at the polar cap edge, and R_E is the earth's radius. This flux should be equal to half of the total geomagnetic flux through the magnetotail, $\pi R_T^2 B_T/2$ where R_T is the tail radius, and B_T is an average tail magnetic flux. $\theta_C = \cos^{-1}[R_T (B_T/B_0)^{1/2}/2\, R_E]$ is 77.1° for B_T = 15 nT and R_T = 20 R_E, 78.8° for B_T = 20 nT and R_T = 15 R_E ,and 75.0° for B_T = 20 nT and R_T = 20 R_E. These latitudes correspond to the noon cusp latitude on the ground in different magnetospheric conditions.

The spatial distribution of the magnetic field depression in the magnetospheric cusp region has been obtained from a large set of Polar magnetometer data observed in 1996–98 (Tsyganenko and Russell, 1999). The magnetic field depression in the noon sector has been derived as the difference between the total magnitude of observed field and the value calculated from the IGRF model. Near the noon meridian, the large magnetic depression (amounting to − 80 nT) is observed only in a narrow latitudinal range in the cusp region at geocentric distances of 5–9 R_E. Hence, the whistler-mode hiss can propagate in the narrow field-aligned cusp plasma down to some geocentric distance below which no cusp magnetic depression exists because of strong geomagnetic field near the Earth. As to the longitudinal dependence of the magnetic field depression in the magnetosphere, it is largest at the noon meridian and it decreases gradually toward the morning and afternoon sides to disappear at ±40°~60° solar magnetic longitudes from the noon meridian. The magnetosheath plasma penetrates into the narrow cusp region of magnetic field depression, so as to form a deep funnel-like diamagnetic polar cusp plasma with a depressed magnetic field inside. Since the magnetic energy density is greater than the kinetic plasma energy density in the outer magnetosphere, a large plasma density gradient exists in the boundary between the narrow cusp plasma region and the surrounding magnetospheric regions. Therefore, the field-aligned narrow cusp plasma acts as a duct for whistler-mode VLF waves. But, this duct structure of the cusp plasma for VLF waves does not exist in the strong geomagnetic region close to the polar ionosphere.

Next, we discuss particle precipitations into the polar cusp region. The cusp, plasma sheet boundary layer, and equatorward section of plasma mantle are characterized by intense low energy (<1 keV) electron precipitations. In the polar cusp, low-energy electron fluxes increase and average electron energies decrease below 200 eV (Carbary

and Meng, 1986b). In the polar cusp ionosphere, highest intensity of the 630.0 nm oxygen line around the noon in the dayside discrete aurora is caused by enhanced precipitation of low energy (<100 eV) electrons without energetic keV electrons (Sandholt *et al.*, 1985). Intense soft electron (30–500 eV) flux was observed together with low-energy ions of 300 eV– 3 keV in the polar cusp, plasmasheet boundary layer, and mantle by the DMSP-F7 (Waterman *et al.*, 1992). The polar/ TIMAS observed fine spatial variations of precipitating protons with latitudinal width of 0.05°, rapid variations of proton flux, and sudden changes of proton energy in the polar cusp region. Such variations and sudden changes in the proton flux and energy result from spatial structures, but not temporal variation in magnetic reconnection (Trattner *et al.*, 1999). Thus, low-energy particle precipitations have fine spatial structures in the polar cusp region as shown by irregular spectra of the polar cusp hiss.

5. Discussion on generation of polar cusp hiss in the magnetospheric cusp region

Irregular *f-t* spectra and fine intensity variations of the polar cusp hiss may be generated by precipitating low-energy electrons of complicated structure. The frequency range of polar cusp hiss may reflect the energy range of precipitating electrons, and its intensity variation depends on a spatial or longitudinal variations of electron precipitations, since the polar cusp hiss is observed over several hours in MLT for a few minutes in UT along the ISIS orbit as shown by Fig. 2. A duration of individual polar cusp hiss in Fig. 2 is about 3 s or spatial scale of 24 km at satellite speed of 8 km/s which is about 0.2° in longitude at satellite altitude of 1170 km and at geomagnetic latitude of 80°. A latitudinal width of the polar cusp hiss region in Fig. 2 is 1.7° between 79.8°S at 1414:20 UT and 81.5°S at 1416:10 UT, April 12, 1978. If the polar cusp hiss propagates from a high altitude source, a latitudinal width difference between the cusp hiss and electron precipitations results from a spread of the cusp hiss waves over the polar ionosphere since the duct-like structure of cusp plasma does not exist in a strong geomagnetic field near the polar ionosphere. The spatial structure of cusp hiss region obtained from changes of the lower cutoff frequency of cusp hiss corresponds to an ionospheric irregularity caused by electron precipitations. In fact, the cusp hiss intensity is very strong near the lower cutoff frequency caused by the LHR reflection in a plasma irregularity as shown by Fig. 2.

Next, we discuss on a generation mechanism of the polar cusp hiss. Ondoh (1990) has shown that the broad-band auroral hiss is caused by the whistler-mode Cerenkov radiation from precipitating inverted-V electrons above a few keV in the polar topside ionosphere. Kasahara *et al.* (1995) have shown that a V-shaped auroral hiss propagates down to a satellite from high altitude magnetosphere. The whistler-mode refractive index of $n^2 = 1+f_P^2 / f\,(f_H \cos\theta - f)$ becomes infinite at a resonant cone angle θ_R since $\cos\theta_R = f/f_H$. The propagation of whistler-mode waves is possible when $\cos\theta > \cos\theta_R$ or $\theta < \theta_R$, where θ is the wave normal angle to the geomagnetic field. Since at altitudes below 10000 km, $f \ll f_H$ for the whistler-mode VLF waves, the frequency of whistler-mode Cerenkov radiation is given by $f = Ef_P^2 \cos\theta$ /250 f_H kHz obtained from the Cerenkov resonance of $c/n = V\cos\theta$, E=250 $(V/c)^2$ keV for energy of electrons with velocity V

parallel to geomagnetic field, and $n^2 = f_P^2 / f_H f \cos\theta$. At altitudes below 10000 km in the polar magnetosphere ($f \ll f_H$), precipitating electrons above a few keV are necessary to generate the whistler-mode VLF Cerenkov radiation for the polar cusp hiss appearing above 2 kHz. But, since the enhancement of low-energy electrons (50 eV–1 keV) and the lowering of electron average energy to below 200 eV occur in the polar cusp ionosphere (Carbary and Meng, 1986a), the whistler-mode VLF Cerenkov radiations above 2 kHz cannot be generated from electrons above a few keV in the polar cusp ionosphere where f is much smaller than a local f_H. The frequency of the whistler-mode Cerenkov radiation for the exact refractive index is given by

$$f = (f_H \cos\theta / 2) \cdot \left[1 \pm \left\{ 1 - (2V f_P / c f_H \sqrt{1 - (V\cos\theta / c)^2})^2 \right\}^{1/2} \right] \text{ , and } E = 250 f (f_H \cos\theta - f) / \cos^2\theta \, [f (f_H \cos\theta - f) + f_P^2]$$

represents the energy of electrons moving parallel to the geomagnetic field where c is the light speed. The term $\sqrt{1-(V\cos\theta/c)^2}$ is approximately equal to 1, and $(2V f_P/cf_H)^2 \ll 1$ in the magnetosphere within 8 R_E. Hence, the frequency of whistler-mode VLF Cerenkov waves is approximately given by $f = f_H \cos\theta$ for the plus sign solution in the outer magnetosphere ($8 \geq L \geq 3$).

In the outer magnetosphere where a local f_H is in the VLF band, we must use this expression for the whistler-mode Cerenkov VLF radiation. The whistler-mode polar cusp hiss at frequencies below 5.8 kHz was simultaneously observed with electrons of 20 eV–1 keV at 1430 UT (13.7 MLT), June 20 (172 days), 1976 by Hawkeye-1 at geomagnetic latitude of 65.0°N and $R = 6.2$ R_E in the cusp magnetospheric region (Gurnett and Frank, 1978) as shown by Fig. 5. Energy spectra of protons and electrons in Fig. 6 were observed together with plasma waves by Hawkeye-1 (Gurnett and Frank, 1978). The ordinate in Fig. 6 is the particle energy in $\log_{10}$(eV) and the time is in UT. The lower panel of Fig. 6 shows that electrons below about 1 keV were observed along with the whistler-mode polar cusp hiss at frequencies below 5.8 kHz of local f_H (Fig. 5) in the cusp magnetospheric region around 6.2 R_E at 1430 UT, June 20, 1976. The range of electron energy observed in high altitude cusp region is consistent with the polar cusp signatures of low-energy electrons observed by the DMSP satellites (Carbary and Meng, 1986a). At the point of latitude 65.0° and $R = 6.2$ R_E, the whistler-mode resonance cone angle is $\theta_R = 26.8°$ for $f = 5.0$ kHz and $f_H = 5.6$ kHz in the geomagnetic field of 200 nT. We estimate the electron energy necessary for generating the 5 kHz whistler-mode Cerenkov radiation at two angles of $\theta = 26°$ and 0° below $\theta_R = 26.8°$ in the above conditions by using the above expressions of frequency and electron energy. Table 1 indicates that whistler-mode Cerenkov 5 kHz waves are generated by electrons below 1 keV in high altitude cusp region, and that the necessary electron energy is lower at wave normal angle near the resonance cone angle than at $\theta = 0°$ for the same electron density. Since an electron beam has a distribution around the Cerenkov resonant velocity, and the whistler-mode refractive index changes in space and time, the Cerenkov resonant condition is continuously kept in some part of the magnetosphere. So, coherent whistler-mode Cerenkov emissions are generated from the electron beam coherently modulated by an interaction between the periodic wave electric field and electron velocity component in the wave normal direction. Whistler-mode Cerenkov VLF waves of different frequencies

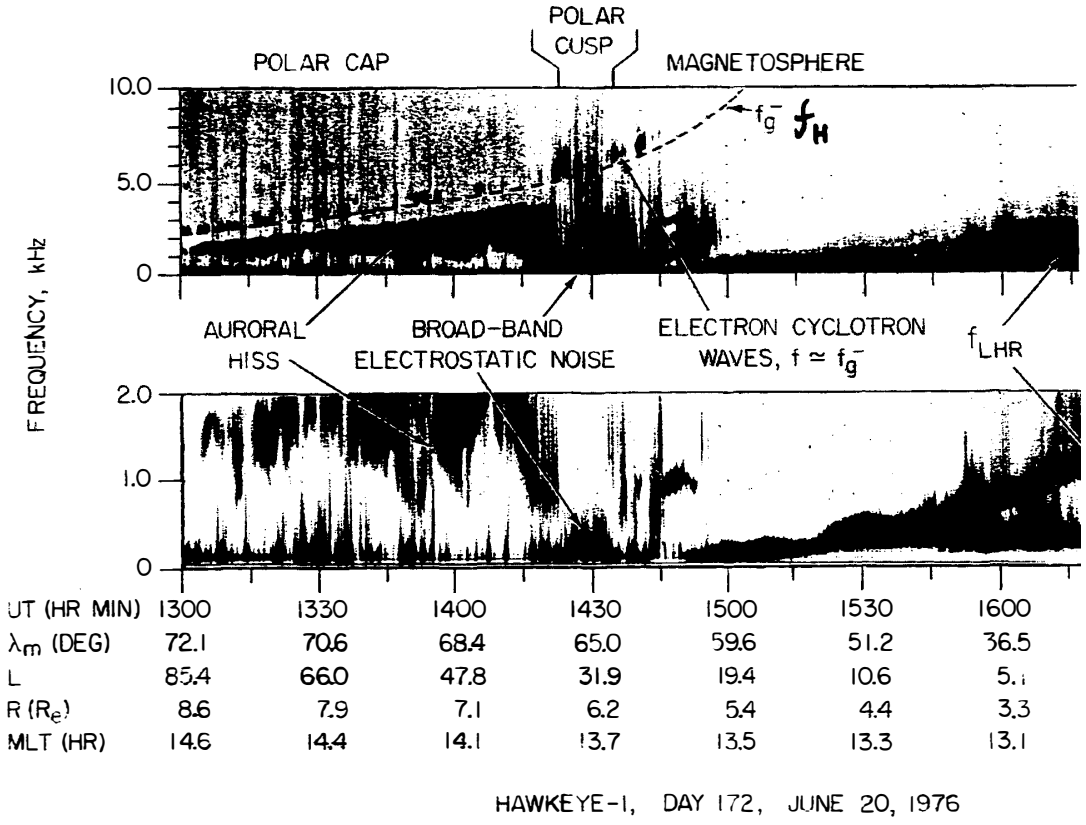

Fig. 5. Plasma wave f-t spectra observed by Hawkeye-1 for 1300–1615 UT, June 20, 1976 at geocentric distances from 8.6–3.3 R_E. Upper and lower panels are in dc-10 kHz and dc-2 kHz, respectively (Gurnett and Frank, 1978), where f_g^- is the electron gyrofrequency, f_H.

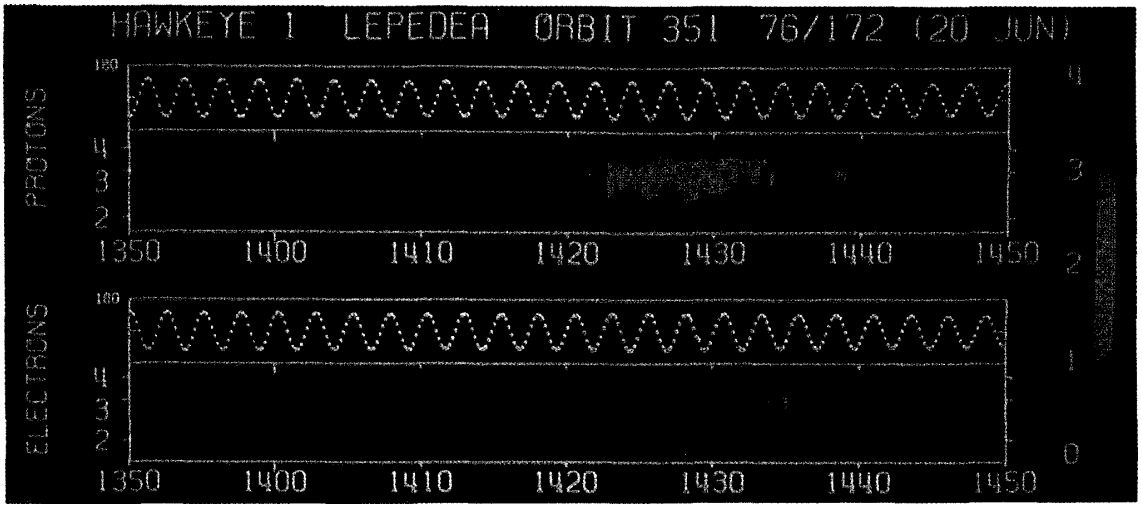

Fig. 6. Energy-time spectrograms of protons (upper panel) and electrons (lower panel) observed simultaneously with plasma waves by Hawkeye-1 for 1350–1450 UT, June 20, 1976 (Gurnett and Frank, 1978); ordinate is the particle energy in $\log_{10}(eV)$.

Table 1. Electron energy for whistler-mode Cerenkov 5 kHz radiation where N is the electron density.

θ=26°	E	63.4 eV	127 eV	1.27 keV
	N	10/cm^3	5/cm^3	0.5/cm^3

θ=0°	E	920 eV	1.84 eV
	N	10/cm^3	5/cm^3

are radiated at different resonant electron velocities in different wave normal directions for the same plasma density and magnetic field. Therefore, the whistler-mode Cerenkov VLF waves of different frequencies are trapped in the cusp plasma duct and propagate as a broad-band cusp hiss in the ducted mode along the field-aligned cusp plasma toward the polar ionosphere, since the whistler-mode propagation condition of $\theta < \theta_R$ is always satisfied by an increase of f_H at lower altitudes as the waves propagate downward. However, such field-aligned structures may exist, at most, down to altitudes of a few thousand km. Even if the cusp hiss propagates in the ducted mode from the high altitude source, the cusp hiss waves spread over the polar ionosphere. Any small-scale structure of the cusp hiss produced in the high altitude source region becomes indistinct in the polar ionosphere by the wave spread effect. The irregular *f-t* spectra of cusp hiss as seen in Figs. 2a–2b represent the spatial dependence of the cusp hiss due to ionospheric irregularities. The ionospheric irregularities in the cusp region are caused by particle precipitations and changing electric fields.

6. Conclusion

The polar cusp hiss observed with ISIS satellites seems to be the whistler-mode VLF Cerenkov waves generated by the low-energy electrons in the high altitude (~6 R_E) cusp region. The cusp hiss generated at high altitudes propagate downward in ducted-mode in the field-aligned cusp plasma with depressed magnetic field. However, the narrow diamagnetic cusp plasma structure does not extend to the lower magnetosphere because the geomagnetic field becomes stronger toward the Earth. Below this region, the cusp hiss waves spread over the ionospheric region. Irregular variations of the lower cutoff frequency of polar cusp hiss seem to reflect spatial plasma irregularities caused by low-energy electron precipitations onto the polar cusp ionosphere.

Acknowledgments

I thank the wintering party members at Syowa Station, Antarctica for their data acquisition from the ISIS satellites.

The editor thanks the referees for their help in evaluating this paper.

References

Carbary, J.F. and Meng, C.-I. (1986a): Correlation of cusp latitude with B_z and AE(12) using nearly one year's data. J. Geophys. Res., **91**, 10047–10054.

Carbary, J.F. and Meng, C.-I.(1986b): Relations between the interplanetary magnetic field Bz, AE index, and cusp latitude. J. Geophys. Res., **91**, 1549–1556.

Gurnett, D.A. and Frank, L.A. (1978): Plasma waves in the polar observations from Hawkeye 1. J. Geophys. Res., **83**, 1447–1462.

Kamei, T. and Maeda, H. (1981): Auroral electrojet indices (AE) for January-June 1978. World Data Center C2 for Geomagnetism Data Book, **3**, 108 p.

Kasahara, Y., Yoshida, K., Matsuo, T., Kimura, I. and Mukai, T. (1995): Propagation characteristics of auroral hiss observed by Akebono satellite. J. Geomagn. Geoelectr., **47**, 509–525.

Kimura, I. (1966): Effects of ions on whistler mode ray tracing. Radio Sci., **1**, 269–283.

Ondoh, T. (1990): Broad-band auroral VLF hiss and inverted-V electron precipitation in the polar magnetosphere. J. Atmos. Terr. Phys., **52**, 385–397.

Ondoh, T. (1997): Characteristics of polar cusp VLF emissions observed by ISIS satellites of low altitude polar orbit. Proc. NIPR Symp. Upper Atmos. Phys., **10**, 50–63.

Ondoh, T., Nakamura, Y. and Murakami, T. (1981): Characteristics of VLF saucers and auroral hiss from ISIS satellites received at Syowa Station, Antarctica. Mem. Natl Inst. Polar Res., Spec. Issue, **18**, 54–71.

Sandholt, P.E., Egeland, A., Holtet, J.A., Lybekk, B., Svenes, K. and Asheim, S. (1985): Large- and small-scale dynamics of the polar cusp region. The Polar Cusp, ed. by J.A. Holtet and D. Egeland. Dordrecht, D. Reidel, 163.

Trattner, K.J., Fuselier, S.A., Peterson, W.K., Sauvaud, J.A., Stenuit, H., Dubouloz, N. and Kovrazhkin, R.A. (1999): On spatial and temporal structures in the cusp. J. Geophys. Res., **104**, 28411–28421.

Tsyganenko, N.A. and Russell, C.T. (1999): Magnetic signatures of the distant polar cusps: Observations by polar and quantitative modeling. J. Geophys. Res., **104**, 24939–24955.

Watermann, J., De La Beaujardière, O. and Newell, P.T. (1992): Incoherent scatter radar observations of ionospheric signatures of cusp-like electron precipitation. J. Geomagn. Geoelectr., **44**, 1195–1206.

(Received September 22, 1999; Revised manuscript accepted February 22, 2000)